Journal of Materials Chemistry

Cite this: *J. Mater. Chem.*, 2012, **22**, 3939

www.rsc.org/materials

PAPER

The effect of a thermo-responsive polypeptide-based copolymer on the mineralization of calcium carbonate†

Wenjie Zhu, Jiaping Lin* and Chunhua Cai

Received 5th October 2011, Accepted 9th December 2011
DOI: 10.1039/c2jm15007g

$CaCO_3$ crystallization behavior was studied in the presence of a thermo-responsive polypeptide copolymer, poly(*N*-isopropyl acrylamide)-*b*-poly(L-glutamic acid) (PNIPAM-*b*-PLGA). At lower temperatures, the copolymer dissolved well and the unimers mediated the formation of rosette-like calcite crystals through a mesoscale assembly process. At higher temperatures, the copolymer self-assembled into micelles with PNIPAM as the core and PLGA as the shell. The micelles mediated the formation of coral-like aragonite fiber clusters at a high micelle concentration, while fewer aragonite fibers were generated at a low concentration and vaterite crystals were obtained instead of aragonite. The time-resolved experiment revealed that the aragonite fibers were formed through a solution–precursor–solid (SPS) process *via* a transient polymer-induced liquid-precursor (PILP) phase. The new findings through the experiments can enrich our existing knowledge of biomimetic mineralization and provide useful information for designing functional materials.

1. Introduction

Biomimetic mineralization is a process which mimics the ways biological systems produce biominerals with well-defined composite structures. Research in this area has attracted considerable attention from both fundamental and applied points of view.[1,2] Recently, particle-based non-classical crystallization pathways were elucidated to explain how complex minerals formed, which include oriented attachment, meso-crystal formation and amorphous precursor particles.[2] The polymer-induced liquid-precursor (PILP) phase was also identified in recent years, which is a highly hydrated and labile precursor phase of minerals.[3] *Via* the PILP process, a variety of morphologies, such as helices,[4] films,[5] and fibers[6–8] were generated. The studies of the crystallization routes can enrich the understanding of the biomineralization process and help to prepare functional materials for biomedical and industrial applications.[9]

Inspired by protein controlled mineralization in organisms, crystallization of inorganics in the presence of proteins and their analogues has been investigated as a model for biomineralization. Natural proteins, such as mollusk shell protein, nacre-associated oyster shell protein, spider silk, and collagen were employed to control mineral crystallization.[10] Researchers have also focused on synthetic hydrophilic polypeptides such as poly(L-glutamic acid) (PLGA), poly(aspartic acid) (PAsp), poly(L-lysine) (PLL) and their derivates because they are structurally simple and easily prepared.[4,11–14] Gower *et al.* found that PAsp can induce the PILP process in calcium carbonate ($CaCO_3$) crystallization to produce a helix superstructure.[4] Yu *et al.* used poly(ethylene glycol)-*b*-poly(L-glutamic acid) to direct $CaCO_3$ crystallization and generate monodisperse vaterite microspheres in mixed solvents of ethanol and water.[12] Yamamoto *et al.* prepared helical $CaCO_3$ superstructures in the presence of copoly[L-(phosphorylated)serine$_{75}$-*block*-aspartic acid$_{25}$].[14] However, most of these polymers are hydrophilic, which are structurally different from mineral proteins because all proteins are generally amphiphilic.

Another strategy in biomimic mineralization is applying organic assemblies of amphiphilic molecules, because they can provide a suitable environment for the controlled nanoscale synthesis of biominerals.[15] It is well known that amphiphilic copolymers can self-assemble into core–shell micelles.[16,17] Although few researches have been concerned with mineralization under control of polymer micelles, it has been shown that polymer micelles are effective modifiers for crystal growth.[18–23] For example, Tam's group investigated poly(ethylene oxide)-*b*-poly(methacrylic acid) (PEO-*b*-PMAA) micelles as a template for the controlled precipitation of calcium phosphate. A nest structure consisting of hybrid nanofilaments was obtained under the control of polymer micelles at low pH value, and the micelles are believed to play an important role in the formation of the

Shanghai Key Laboratory of Advanced Polymeric Materials, State Key Laboratory of Bioreactor Engineering, Key Laboratory for Ultrafine Materials of Ministry of Education, School of Materials Science and Engineering, East China University of Science and Technology, Shanghai, 200237, China. E-mail: jlin@ecust.edu.cn; jplinlab@online.sh.cn; Fax: +86-21-64251644; Tel: +86-21-64253370

† Electronic supplementary information (ESI) available: ^{1}H NMR spectra and scattered intensity–temperature curve of NG192 block copolymers, SEM images of $CaCO_3$ samples controlled by PNIPAM, PLGA polymers and NG micelles and the corresponding FT-IR spectra. See DOI: 10.1039/c2jm15007g

intriguing structure.[19] Yu *et al.* prepared a ringlike $CaCO_3$ superstructure by using aggregates of hydrophobically modified poly(ethylene glycol)-*b*-poly(ethylene imine)-poly(acetic acid). The mechanism is based on a formation of $CaCO_3$ nanoparticles in the polymer assemblies and subsequent aggregation of the nanoparticles. As the polymer contains chelating units, this leads to the selective dissolution of the core of the particle and microrings were finally formed.[20] Lee *et al.* prepared spatially mineralized poly(ethylene glycol)-*b*-poly(L-aspartic acid)-*b*-poly(L-phenylalanine) micelles with calcium phosphate nanoshells. The hybrid nanocarriers were used for the controlled release of an anticancer drug.[21] In the examples mentioned above, the micelles all served as mineralization templates.

Polymer micelles can also play a significant role in the formation of amorphous minerals. Meldrum *et al.* reported that $CaCO_3$ fibers which grow on glass and mica initially occur by the formation of a copolymer-stabilised amorphous calcium carbonate (ACC) phase. It was found that the polymers formed aggregates at low pH values prior to fiber growth.[23] So far, polymer micelle controlled mineralization has not been fully investigated, and more experiments are needed to explore the role of polymer micelles in the formation of amorphous or liquid precursors of minerals.

In this work, $CaCO_3$ crystallization behavior under the control of poly(*N*-isopropyl acrylamide)-*b*-poly(L-glutamic acid) (PNIPAM-*b*-PLGA) copolymers was studied. PNIPAM is a well known thermoresponsive polymer, which exhibits a lower critical solution temperature (LCST) in aqueous solution. The PNIPAM-*b*-PLGA copolymers can self-assemble into micelles above the LCST in basic solution. The effects of the unimers and micelles on the crystallization of $CaCO_3$ were studied respectively. The morphology and polymorph of $CaCO_3$ samples were investigated by field emission scanning electron microscopy (FE-SEM) and X-ray diffraction (XRD) as well as Fourier transform infrared spectroscopy (FT-IR). It was discovered that the unimers mediated the formation of rosette-like calcite, while polymer micelles mediated the formation of aragonite fibers and vaterite particles. With the aid of a series of control experiments and time-resolved experiments, the mechanisms regarding the unimer- and micelle-controlled mineralization were proposed.

2. Experimental section

2.1 Materials

N-isopropylacrylamide (NIPAM, 97%, Aldrich) was purified by recrystallization from *n*-hexane. 2, 2′-Azobisisobutyronitrile (AIBN, CR) was recrystallized from absolute ethanol. 2-Aminoethanethiol hydrochloride (AET·HCl) was purchased from Aldrich and used without further purification. γ-Benzyl-L-glutamate-*N*-carboxyanhydride (BLG-NCA) was synthesized according to the procedures reported in the literature.[24] $(NH_4)_2CO_3$ and $CaCl_2$ and other chemicals were of analytical grade and used as received. Deionized water (DIW) was made in a Millipore Super-Q Plus Water System to a level of 18.2 MΩ cm resistance. All glassware for crystallization (glass bottles and small pieces of glass substrates) was cleaned and sonicated in ethanol for 5 min. It was then rinsed with DIW and further soaked in a H_2O–HNO_3(65%)–H_2O_2 (1 : 1 : 1, v/v/v) solution, and then rinsed with DIW, and finally dried in air with acetone.

2.2 Synthesis of block copolymers

Monoamino-terminated PNIPAM (PNIPAM–NH_2) was synthesized by the free radical polymerization of NIPAM in methanol at 60 °C using AIBN as the initiator and AET·HCl as the chain transfer reagent.[17,25] The number of repeat units and polydispersity index (PDI) of PNIPAM were 45 and 1.57, respectively, tested by gel permeation chromatography (GPC) using THF as eluent and calibrated with polystyrene standards. PNIPAM-*b*-PBLG copolymers were synthesized by ring-opening polymerization of γ-benzyl-L-glutamate-*N*-carboxyanhydride (BLG-NCA) initiated by the PNIPAM–NH_2 in anhydrous 1,4-dioxane. The composition of the PNIPAM-*b*-PBLG copolymer was determined from ^{1}H NMR spectra (Fig. S1†). The polydispersity index (PDI) of PNIPAM-*b*-PBLG was determined by GPC in dimethylformamide (DMF). PNIPAM-*b*-PLGA block copolymers were prepared by hydrolyzation of PNIPAM-*b*-PBLG with potassium hydroxide (KOH).[26] The deprotection of the benzyl group was confirmed by the disappearance of the methylene proton peak (5.1 ppm) of the PBLG block in the NMR spectra (Fig. S1b†).

2.3 Preparation of polymer micelles

The copolymer micelle solution was prepared by directly dissolving PNIPAM-*b*-PLGA copolymers in basic aqueous solution and then raising the temperature of solution. In a typical procedure, 40 mg PNIPAM-*b*-PLGA was dissolved in 10 mL DIW firstly by the aid of sonication and NaOH. Then 22 mg (0.20 mmol) $CaCl_2$ was added as the calcium source of $CaCO_3$. The pH value of the solution was carefully adjusted to about 8.0 by NaOH, HCl and DIW. The final solution volume was fixed at 20 mL. Then the solution was filtered by using a 0.22 μm Millipore to remove impurities. To prepare micelles, the solution was put in a 50 °C constant temperature oven for 24 h.

2.4 Mineralization

The mineralization was performed by a gas-diffusion method as described by Addadi *et al.*[27] Firstly, 5 mL of the polymer solution and some glass wafers were put in a 10-mL bottle. The bottle was covered by pierced parafilm and placed at a 5 L desiccator in a constant temperature oven. After that, 6 g $(NH_4)_2CO_3$ in another bottle was placed at the bottom of the desiccator. For a certain time (typically 72 h at 25 °C, 24 h at 40 and 50 °C), the glass wafers were taken out, and rinsed with DIW, then dried in air for further characterization.

2.5 Measurements

Scanning electron microscopy (SEM). The samples on the glass wafers were observed by scanning electron microscopy (SEM) (JSM-6460, JEOL) operated at an accelerating voltage of 10 kV. Before the observation, the samples on the glass wafers were sputtered with carbon.

High-resolution transmission electron microscopy (HR-TEM) and selective area electronic diffraction (SAED). The HR-TEM and SAED analyses were performed on a JEM-2100F HR-TEM operated at an accelerating voltage of 200 kV. The crystals were scraped from the glass wafers and dispersed in water. Then, the sample was transferred to a copper grid with carbon film and dried in air before observation. SAED was used to learn whether the crystal was single crystalline or polycrystalline.

Optical microscopy (OM). An optical microscope was used to observe the morphology of samples in glass wafers in the crystallization process. The glass wafer was observed immediately after being taken from the glass bottle. The optical microscope micrographs were taken with an Olympus BH-2 optical microscope.

X-ray diffraction (XRD). XRD was used to analyze the crystalline structure. XRD patterns were recorded on Rigaku D/Max-2550V with Cu-Kα radiation.

Fourier transform infrared spectroscopy (FT-IR). For FT-IR analysis, the samples were pressed with KBr into pellets. The spectra of the samples were recorded on a Nicolet 5700 FT-IR spectrometer in transmission mode.

Laser light scattering measurements (LLS). LLS experiments involving dynamic light scattering (DLS) and static light scattering (SLS) were performed using an ALV laser goniometer, with a 22 mW linearly polarized He-Ne laser ($\lambda = 632.8$ nm) and an ALV-5022 multiple tau digital correlator. The measurements were taken at a fixed angle 90°. The DLS was used to detect changes of apparent sizes for the aggregates. The SLS was used to monitor the aggregation process of the PNIPAM-*b*-PLGA solution in the process of heating.

3. Results

3.1 Characterization of PNIPAM-*b*-PLGA and the micellizaion behavior

The PNIPAM-*b*-PLGA copolymers were prepared by ring-opening polymerization of γ-benzyl-L-glutamate-*N*-carboxy-anhydride (BLG-NCA) initiated by PNIPAM-NH_2 followed by deprotection of the benzyl groups. Detailed information regarding the characteristics of the polymers is provided in Table 1. Three copolymers denoted as NG192, NG42 and NG12 were prepared, where the "192", "42" and "12" denote the PLGA repeating units.

Table 1 The characteristics of PNIPAM-*b*-PLGA copolymers

Sample	Copolymer[a]	M_n[b]	PDI[c]
NG192	$PNIPAM_{45}$-*b*-$PLGA_{192}$	47140	1.17
NG42	$PNIPAM_{45}$-*b*-$PLGA_{42}$	14300	1.32
NG12	$PNIPAM_{45}$-*b*-$PLGA_{12}$	7720	1.51

[a] The composition of the copolymers is derived from ^{1}H NMR spectra of the precursor PNIPAM-*b*-PBLG in $CDCl_3$/TFA mixed solvents. [b] The number-average molecular weights M_n of the precursor PNIPAM-*b*-PBLG are calculated from the composition given in the second column. [c] The polydispersity indices (PDI), M_w/M_n (M_w is the weight-average molecular weight and M_n is the number-average molecular weight) of the precursor PNIPAM-*b*-PBLG are determined by GPC.

The three copolymers can be dissolved well in basic solution and the solution is clear at room temperature. The PNIPAM block becomes insoluble above the LCST. As a result, the copolymers self-assemble into aggregates causing the aqueous system to turn cloudy. SLS was employed to characterize the self-assembly behavior of NG_{192}. The temperature dependence of scattering light intensity is plotted in Fig. S2.† The scattered intensity is very weak below 33 °C. Above 33 °C micellization starts to occur, as indicated by the dramatic increase in scattered intensity. Fig. 1 displays the TEM images of micelles formed by the three copolymers at 50 °C. The NG192 copolymers form spherical micelles at concentrations of (C_{NG192}) of 2.0 and 0.1 g L^{-1} as shown in Fig. 1a and b, respectively. As the length of PLGA decreases, the aggregate morphology transforms to rods (Fig. 1c) and then to vesicles (Fig. 1d). In the present work, we evaluated the effects of unimers and aggregates on the $CaCO_3$ crystallization at 25 °C (below the LCST) and 50 °C (above the LCST) as typical temperatures.

3.2 $CaCO_3$ crystallization in the presence of PNIPAM-*b*-PLGA unimers below the LCST

Double-hydrophilic block copolymers (DHBCs) have been widely used as an effective additive for the control of the morphology of $CaCO_3$.[2] Typically, a DHBC consists of a binding block designed to interact strongly with the surfaces of inorganic minerals, and a second solvating block that does not interact but mainly promotes solubilization in water. The PLGA block is a binding block which could interact with minerals owing to the carboxyl groups in the chain.[11,12] At 25 °C, the PNIPAM block

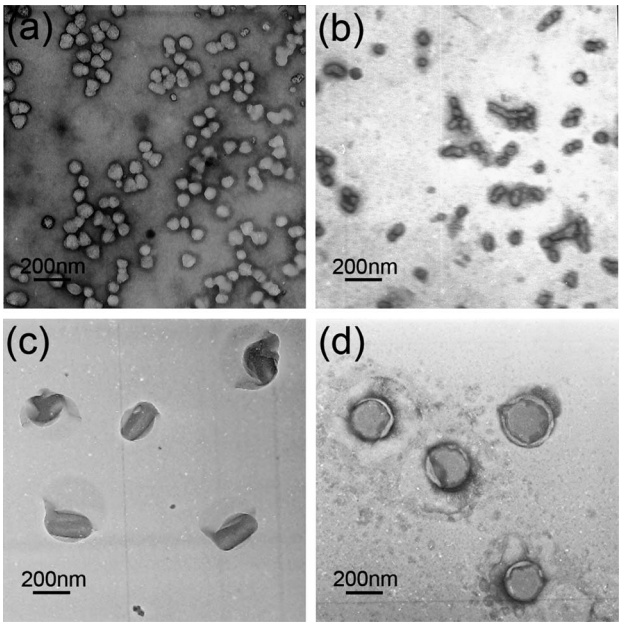

Fig. 1 TEM images of PNIPAM-*b*-PLGA aggregates self-assembled in aqueous solution at 50 °C: (a) spherical micelles, $C_{NG192} = 2.0$ g L^{-1}, (b) spherical micelles, $C_{NG192} = 0.1$ g L^{-1}, (c) rod micelles, $C_{NG42} = 2.0$ g L^{-1}, (d) vesicles, $C_{NG12} = 2.0$ g L^{-1}.

can be regarded as a solvating block since it interacts weakly with $CaCO_3$ minerals.[28] The effects of $PNIPAM_{45}$ and $PLGA_{274}$ homopolymers on the $CaCO_3$ crystallization were examined at 25 °C (see Fig. S3, ESI†). With $PNIPAM_{45}$ as the additive, the formed crystals exhibit a typical rhombohedral structure (Fig. S3a†), which is similar to the crystals formed in the absence of polymers. This indicates that $PNIPAM_{45}$ only have a weak effect on $CaCO_3$ mineralization. When $PLGA_{274}$ was used as the additive, rosette-like crystals were obtained (Fig. S3c†).

The effect of NG192 copolymers on the $CaCO_3$ crystallization was investigated at 25 °C after 72 h of reaction. As shown in Fig. 2a, the $CaCO_3$ crystals in 1.0 g L^{-1} solution have rosette-like structures, which are approximately 20 μm spheres with their surfaces composed of rhombohedral subunits. The morphology of crystals grown in 0.1 g L^{-1} polymer solution is similar to those prepared in 1.0 g L^{-1} solution, while the dimension of the subunits become bigger (Fig. 2b). The samples are principally calcite from the FT-IR spectroscopy measurement with the feature peaks of the calcite phase at 712 and 874 cm^{-1} (Fig. S4,† ESI). In the cases of NG42 and NG12 solutions, the $CaCO_3$ morphology (not shown) is also rosette-like, similar to that prepared in NG192 solution.

$CaCO_3$ rosette-like crystals have been widely reported under the control of various kinds of DHBCs[29,30] and biopolymers.[31,32] The formation of such rosette-like crystals arises from a meso-scale self-assembly process in these systems.[30,31] The rosette-like crystals can be viewed as aggregates of building units formed in the prior stage. The PLGA blocks are able to interact with the building units and the PNIPAM blocks could provide the water solubility of the units. Therefore, the building units can be temporarily stabilized by the copolymers. During the growing process, the building blocks do not stack regularly due to the repulsive interaction of the polymer chains, thus leading to the rosette-like crystal formation after their aggregation.[30]

3.3 $CaCO_3$ crystallization in the presence of PNIPAM-*b*-PLGA micelles above the LCST

When the temperature is above the LCST, the PNIPAM-*b*-PLGA copolymers self-assemble into micelles. The micelle solution shows a distinct effect on the $CaCO_3$ crystallization. Fig. 3 presents SEM and TEM images of $CaCO_3$ precipitates obtained in the presence of 2.0 g L^{-1} micelle solution at 50 °C. The formed structures exhibit a hierarchical coral-like cluster

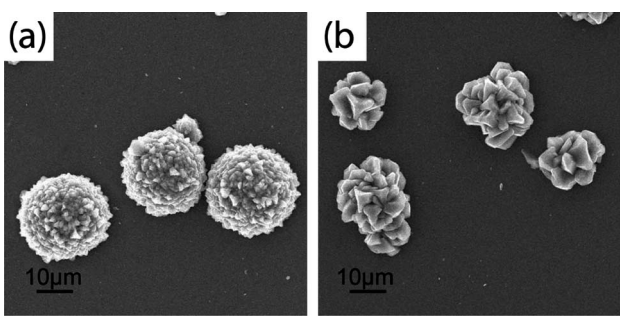

Fig. 2 SEM images of $CaCO_3$ crystals formed in the presence of different concentrations of PNIPAM-*b*-PLGA unimers at 25 °C: (a) 1.0 g L^{-1}, (b) 0.1 g L^{-1}.

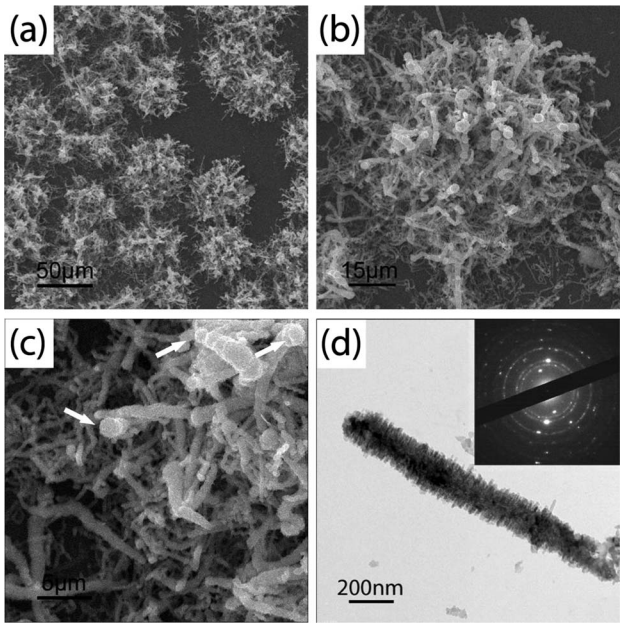

Fig. 3 SEM and TEM images of the sample prepared in the presence of 2.0 g L^{-1} NG192 micelles at 50 °C after 24 h of reaction. The concentration of $CaCl_2$ is 10 mM. Arrows in Fig. 3c indicate the growth tips. The inset in Fig. 3d is the SAED pattern of the fiber.

appearance with diameters of about 50 μm (Fig. 3a). Close inspection of the cluster structures reveals that the coral-like structures are composed of fibers with diameters ranging from 0.2 to 2.0 μm and lengths up to tens of micrometres (Fig. 3b, c). Most fibers are not straight and usually grow in a serpentine fashion. Drop-like growth points can be frequently seen at the tip of some fibers as indicated by the arrows. Fig. 3d shows a typical TEM photograph of a fiber. The fiber has a diameter of about 200 nm and is covered with a large number of nanorods about 15 nm in diameter. The nanorods grow perpendicularly and are densely aligned in parallel to one other. Although the nanorods are organized to some degree, the SAED pattern displays obvious rings, as shown in the inset of Fig. 3d, indicating that the structure of the fiber is polycrystalline.

The polymorph of the sample was examined by XRD and FT-IR measurements. The results are shown in Fig. 4. The XRD pattern of the crystals exhibits sharp reflections at 0.339, 0.327, 0.270, 0.247, 0.237, 0.233 and 0.197 nm, which are consistent with the (111), (021), (012), (200), (112) and (022) reflections of aragonite (Fig. 4a). No peak of calcite or vaterite can be found, indicating the sample is nearly pure aragonite. This was further confirmed by the FT-IR spectra by the presence of only the 700 and 712 cm^{-1} (ν4 mode), and 858 cm^{-1} (ν1 mode) CO_3^{2-} absorption bands of a typical aragonite phase (Fig. 4b).[33]

The aragonite fibers can be obtained at a wide range of temperatures above the LCST in the copolymer solution. For example, we examined the morphology and polymorph of the samples obtained at 40 °C (Figs S5 and S6,† ESI). Similar to the samples prepared at 50 °C, aragonite fiber is the predominant morphology in 2.0 g L^{-1} micelle solution at 40 °C. We also prepared the $CaCO_3$ crystals in the presence of PNIPAM or PLGA homopolymers as a control experiment. It was found that

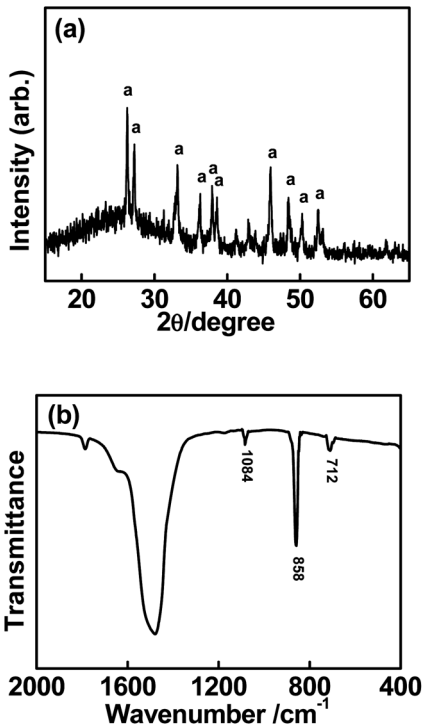

Fig. 4 XRD patterns (a) and FT-IR spectra (b) of the $CaCO_3$ crystals formed in the presence of 2.0 g L^{-1} NG192 at 50 °C after 24 h of reaction. Note: the letter "a" denotes aragonite (JCPDS: 41-1475).

the influence of the homopolymers on the $CaCO_3$ crystallization is independent of the experimental temperature. For example, the $PNIPAM_{45}$ and $PLGA_{274}$ homopolymers mediate the formation of rhombohedral and rosette-like crystals, respectively, at higher temperature, which appear identical to those prepared at 25 °C (Figs S3b, d,† ESI). Thus, it can be concluded that the PNIPAM-*b*-PLGA micelles play a crucial role in the formation of aragonite fibers.

We found that the micelle concentration is another factor which influences the mineralization. In the studies of this effect, we prepared micelle solutions with concentrations of 1.0, 0.3 and 0.1 g L^{-1} to mediate $CaCO_3$ precipitation. Fig. 5 shows the SEM images of crystals obtained from the solutions with various concentrations. Similar to the $CaCO_3$ formed in 2.0 g L^{-1} micelle solution (Fig. 3), the structures are mostly clusters of fibers under control of 1.0 g L^{-1} micelle solution (Fig. 5a, b). Lowering the micelle concentration to 0.3 g L^{-1}, we found that both fibers and irregular particle aggregates exist (Fig. 5c, d). The typical dimensions of the particles are in the micron range. When the concentration of the micelle solution is further decreased to 0.1 g L^{-1}, the particles are the majority and fibers are very few (Fig. 5e, f).

The polymorph of the three $CaCO_3$ samples formed in the micelle solutions with different concentrations was examined by XRD measurement (Fig. 6). As mentioned above, the sample formed in 2.0 g L^{-1} micelle solution is pure aragonite. For the samples in 1.0 and 0.3 g L^{-1} polymer solutions, the polymorphs are indexed as a mixture of aragonite and vaterite (Fig. 6a, b). Further decreasing the micelle concentration to 0.1 g L^{-1}, we find that only weak peaks of aragonite polymorph can be seen in the XRD figure, indicating that the crystals are mainly vaterite (Fig. 6c).

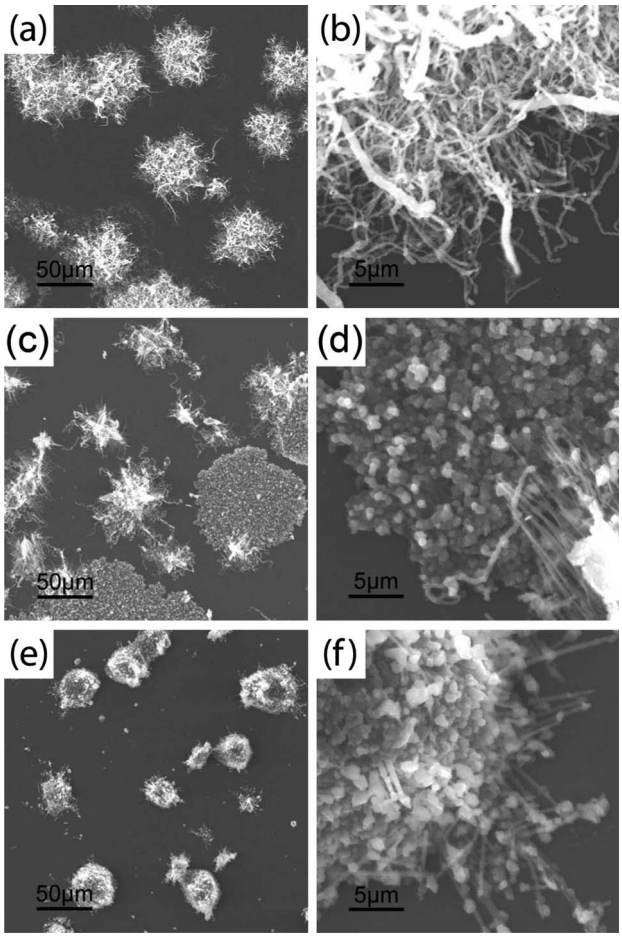

Fig. 5 SEM images of $CaCO_3$ crystals formed in the presence of NG192 with various micelle concentrations at 50 °C after 24 h of reaction: (a, b) coral-like structure in 1.0 g L^{-1} NG192 micelle solution, (c, d) fibers and particles in 0.3 g L^{-1} NG192 micelle solution, (e, f) particles and few fibers in 0.1 g L^{-1} NG192 micelle solution.

The FT-IR spectra were also recorded for the $CaCO_3$ products to complement the XRD results (Fig. 7). The vibration bands at *ca.* 745 and 877 cm^{-1} can be attributed to the ν4 (in-plane bending mode) and ν2 (out-of-plane bending mode) bands of

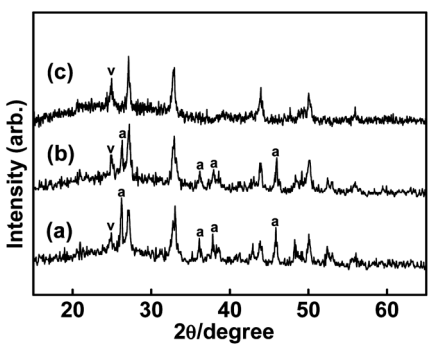

Fig. 6 XRD patterns of the $CaCO_3$ crystals prepared in the presence of NG192 micelle solutions with various concentrations at 50 °C after 24 h of reaction: (a) 1.0 g L^{-1}, (b) 0.3 g L^{-1}, (c) 0.1 g L^{-1}. Note: the letter "a" denotes aragonite (JCPDS: 41-1475), the letter "v" denotes vaterite (JCPDS: 72-0506).

vaterite.[33] The feature peaks of vaterite become more and more evident with decreasing the micelle concentration. This is in good agreement with the XRD results as shown in Fig. 6. The above results indicate that a lower micelle concentration favors vaterite formation.

The effect of block copolymer composition on the $CaCO_3$ crystallization was also evaluated by replacing NG192 with NG12 and NG42. Rosette-like calcite crystals were observed for both NG12 and NG42 samples at 25 °C. At 50 °C, the SEM images of the two crystal samples formed in NG12 and NG42 micelle solutions with a concentration of 2.0 g L^{-1} are shown in Fig. 8. The main parts are clusters consisting of needle-like crystals. Compared with the sample formed in NG192 micelle solution (Fig. 3), fewer fibers could be observed, and aragonite and vaterite coexist in the crystals as determined from the FT-IR spectra (Fig. S7†). The result indicates that the PNIPAM-*b*-PLGA copolymers with a short PLGA chain length are unfavorable for mediating the formation of the aragonite fibers.

3.4 Time-resolved experiment of the crystal formation in the presence of NG192 micelles

Fibrous inorganic minerals can be produced in the presence of polymers through several ways, *e.g.* anatase chain structures *via* oriented attachment,[34] $BaCO_3$ helices *via* polymer-coded assembly of short nanorod tectons,[35] and hydroxyapatite filaments *via* site-selective growth.[18] Recently, it was reported that calcite fibers, $BaCO_3$ fibers and helices were produced *via* a so-called solution–precursor–solid (SPS) mechanism associated with the PILP process.[6,7] In the process, a "molten flux droplet" is created from the PILP droplets, which contains a high concentration of ionic reactants. The crystal is then restricted to one-dimensional growth by the size of the flux droplets. A fiber grows continuously as long as the flux droplet is replenished with reactants.[3] The SPS process has characters of liquid–liquid phase separation in the crystallizing solution and drop-like growth points at the tip of fibers.

In the present work, the crystallization of $CaCO_3$ under control of NG192 micelles shows characters of the SPS process. To clarify the mechanism of the fiber formation, a time-resolved experiment was performed in the mineralization system with 2.0 g L^{-1} NG192 at 50 °C. Fig. 9 displays the evolution of $CaCO_3$ morphologies at different intervals. After 90 min crystallization,

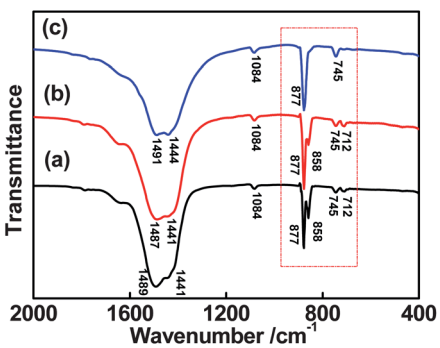

Fig. 7 FT-IR spectra of $CaCO_3$ crystals prepared in the presence of NG192 micelle solutions with various concentrations at 50 °C after 24 h of reaction: (a) 1.0 g L^{-1}, (b) 0.3 g L^{-1}, (c) 0.1 g L^{-1}.

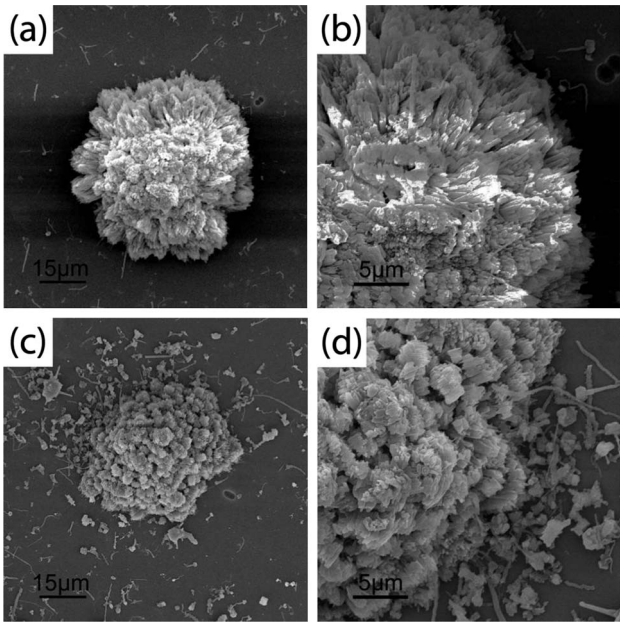

Fig. 8 $CaCO_3$ crystals formed in NG12 (a, b) and NG42 (c, d) micelle solutions at a concentration of 2.0 g L^{-1} at 50 °C.

the solution became rather cloudy. The sample was then observed under optical microscopy. The image shows that the solution contains many mineral droplets with diameters about several micrometres (Fig. 9a). The wetting and coalescence behavior of the micro-droplet indicates the liquid-like character of the $CaCO_3$ precursor phase. Some droplets are amorphous as judged from the lack of birefringence. A birefringent appearance

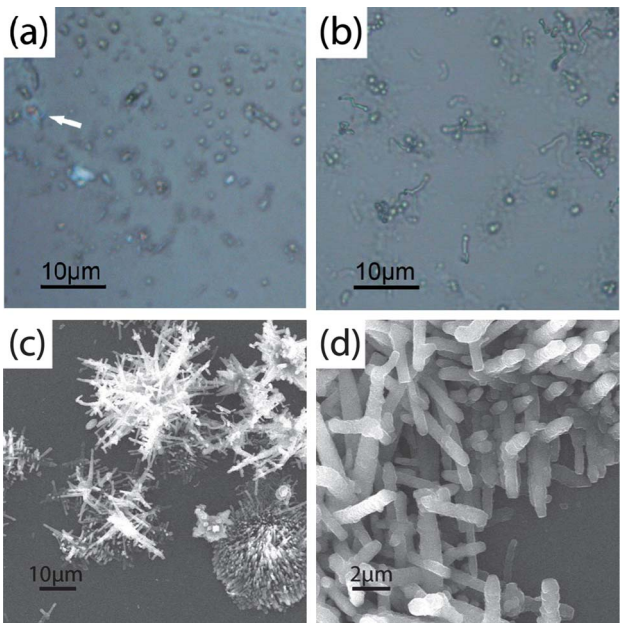

Fig. 9 The morphology evolution of aragonite fibers formed in the early stage. (a) An optical image of liquid precursors for 90 min reaction. (b) An optical image of tiny fibers for 120 min reaction. (c, d) SEM images of the fibers after 5 h of reaction. Arrows in Fig. 9a indicate a crystalline part.

of a crystalline part indicates that these precursors have partially crystallized (as indicated by the arrow). Fig. 9b shows the image of sample which was obtained after 120 min crystallization. Tiny fibers with a curved morphology can be found and almost each one has a spherical "bubble" at the tip. The formed fibers are crystalline as judged from the birefringence behavior, and the diameters of the droplets are much larger than those of fibers. This could be caused by the shrinkage of the highly hydrated droplets when they crystallize into fibers. After 5 h of reaction, clusters of branched fibers can be observed (Fig. 9c, d). The structure is similar to the final crystals after 24 h of reaction. The amorphous droplets at the initial reaction period and droplet-like growth tips on the fibers imply the existence of a PILP phase in the mineralization system.[6–8,36]

The development of the PILP droplets at an early stage in the crystallization was further studied by light scattering. Fig. 10 shows that the diameters of aggregates drastically increase when the reaction proceeds. The increase in the diameters suggests that the liquid precursors are formed through a self-assembly process by the aggregation of micelles. A remarkable character of the micelles is that the corona has a high density of carboxyl groups. For the interaction between COO^- and Ca^{2+}, the corona of micelles can sequester Ca^{2+} with a high localized concentration to form a complex. The high density of carboxyl groups could stabilize amorphous $CaCO_3$ in the corona. As a result, the hydrophilicity of the corona decreases remarkably. Thus the micelles with formed amorphous $CaCO_3$ fuse together due to the van der Waals interactions after repeated particle collisions.

4. Discussion

From the extensive experimental results, we learned that the influences of PNIPAM-*b*-PLGA unimers and micelles on $CaCO_3$ crystallization are distinct. Below the LCST of the PNIPAM block, the PNIPAM-*b*-PLGA copolymer in the unimer state is a type of DHBC, which could stabilize the primary particles transformed from unstable ACC.[30] The primary particles further construct rosette-like crystals through disordered aggregation. At temperatures above the LCST, the formed micelles stabilize the ACC precursor phase in the PILP system and dictate the short-range structures of ACC within the Micelle-ACC.[37] In the system, micelles have a high local concentration of COO^- in the corona, which can sequester and concentrate ionic species around the micelles, while delaying the nucleation of $CaCO_3$ long enough to generate the PILP phase.

The growth of fibers from the PILP phase, as observed, went through a SPS process as revealed by the time-resolved experiment (see Fig. 9), as Scheme 1 shows. Initially, PILP droplets formed in solution due to the interactions among calcium ions, carbonate ions and the micelles (Scheme 1a, b). With more carbonate ions added, some liquid precursors firstly deposit and solidify as Scheme 1c shows. It has been reported that the precursor droplets do not prefer to deposit on a smooth glass surface, but usually are adsorbed onto salient tips such as the rough substrate, fiber ends, or even edges of crystals due to the high surface energy.[5,7,8,38] The droplets can be temporarily stabilized because the copolymers could delay the crystallization. With more reagents continuously diffusing into them, the droplets coalesce and solidify on the tips. When they crystallize, they serve as new end tips for anisotropic growth. Continuous addition of liquid precursors and subsequent crystallization result in the formation of fibers (Scheme 1d). Since defects on formed fibers can also serve as depositing places, branched fibers can be seen as shown in Fig. 9d.

It should be noted that liquid precursors can also be observed at a lower micelle concentration (0.1 g L^{-1} as an example), although fewer fibers are obtained in this case (Fig. 5e,f). This suggests that a low concentration of polymer could not induce the SPS process efficiently. The solution crystal nucleation is less inhibited at a low concentration of copolymers, and thus the liquid precursors crystallize directly without going through the SPS process.

The NG192, NG42 and NG12 block copolymers have the same PNIPAM block chain length but different PLGA chain lengths. The morphologies of formed crystals transform from fiber clusters to large aggregates with decreasing PLGA chain length (see Fig. 3 and Fig. 8). In the NG42 and NG12 copolymers, the mass fraction of PLGA chains is much lower than the NG192 copolymer, and thus the total hydrophilicity of their assemblies is lower than the NG192 copolymer. The PLGA chain length has a close relationship with the colloidal stability of PILP droplets. In the NG192 system, the PILP droplets are more stable because of the long hydrophilic PLGA chains in the micelle coronas. While for the NG42 and NG12 system, the droplets

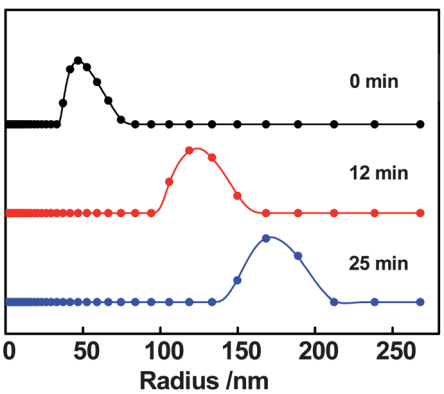

Fig. 10 The evolution of the hydrodynamic radius of particles during the initial reaction period: (a) 0 min, (b) 12 min, (c) 25 min. The hydrodynamic radius was measured by DLS at a fixed angle of 90°.

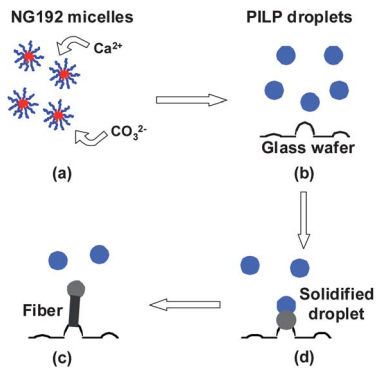

Scheme 1 A schematic image showing the growth of an aragonite fiber through the proposed SPS process.

tend to agglomerate and sedimentate rapidly. The dispersed PILP droplets in the solution contribute to the fiber growth through the SPS process. Therefore long fibers are predominant in the NG192 system, while the crystallization of the deposited PILP phase leads to the formation of large aggregates in NG42 and NG12 system.

In nature, anhydrous calcium carbonate has three crystalline forms. The most thermodynamically stable phase is calcite, followed by aragonite and vaterite. The final crystal habit can be affected by additives due to a shift in the kinetic/thermodynamic balance.[39] In the micelle solution, aragonite phase is formed at a higher concentration, while $CaCO_3$ is inclined to form vaterite upon a decrease of the concentration. The conversion is caused by the different crystallization patterns. Aragonite could hardly homogeneously nucleate under standard conditions. Compared with homogeneous nucleation, the heterogeneous nucleation could reduce the activation energy barrier for aragonite formation.[40] As discussed above, the aragonite fibers are formed *via* the SPS mechanism. The SPS process employing high surface energy regions as nucleation locations may provide suitable conditions for heterogeneous nucleation of aragonite. While a lower micelle concentration militates against the SPS process since homogeneous nucleation is less inhibited. In this pathway, the kinetic stabilization of vaterite is achieved due to the high nucleate rate and stabilization effect of PLGA blocks.

5. Conclusions

In the present work, we studied the unique influence of PNIPAM-*b*-PLGA copolymers on $CaCO_3$ crystallization. The $CaCO_3$ crystallization undergoes different pathways in the presence of PNIPAM-*b*-PLGA block copolymers below and above the LCST of PNIPAM. Below the LCST, the copolymer unimers regulate the growth of rosette-like calcite through a mesoscale self-assembly process. Above the LCST, the PNIPAM-*b*-PLGA copolymers self-assemble into micelles. The copolymer micelles and inorganic ions form amorphous liquid precursors and then grow into aragonite fibers through the SPS process. However, the copolymers with a low concentration or short PLGA length militate against the SPS process and fewer fibers can be obtained. The new findings gained from experiments can not only lead to a better understanding of the PILP process, but also provide useful information for designing novel inorganic materials with fibrous structures.

Acknowledgements

This work was supported by National Natural Science Foundation of China (50925308), Program for Changjiang Scholars and Innovative Research Team in University (No. IR T0825), and National Basic Research Program of China (No. 2012CB933602). Supports from projects of Shanghai municipality (08DZ2230500 and B502) are also appreciated.

Notes and references

1 S. Mann, *Biomineralization: principles and concepts in bioinorganic materials chemistry*, Oxford University Press, Oxford, 2001; A. M. Belcher, X. H. Wu, R. J. Christensen, P. K. Hansma, G. D. Stucky and D. E. Morse, *Nature*, 1996, **381**, 56; G. Falini, S. Albeck, S. Weiner and L. Addadi, *Science*, 1996, **271**, 67.
2 A. W. Xu, Y. Ma and H. Colfen, *J. Mater. Chem.*, 2007, **17**, 415; H. Cölfen, *Top. Curr. Chem.*, 2007, **271**, 1.
3 L. B. Gower, *Chem. Rev.*, 2008, **108**, 4551.
4 L. A. Gower and D. A. Tirrell, *J. Cryst. Growth*, 1998, **191**, 153.
5 Y. Y. Kim, E. P. Douglas and L. B. Gower, *Langmuir*, 2007, **23**, 4862.
6 M. J. Olszta, S. Gajjeraman, M. Kaufman and L. B. Gower, *Chem. Mater.*, 2004, **16**, 2355; S. J. Homeijer, R. A. Barrett and L. B. Gower, *Cryst. Growth Des.*, 2010, **10**, 1040; W. Zhu, C. Cai and J. Lin, *Acta Polym. Sin.*, 2011, **4**, 335.
7 J. H. Zhu, J. M. Song, S. H. Yu, W. Q. Zhang and J. X. Shi, *CrystEngComm*, 2009, **11**, 539.
8 J. H. Zhu, S. H. Yu, A. W. Xu and H. Colfen, *Chem. Commun.*, 2009, 1106.
9 J. Song, V. Malathong and C. R. Bertozzi, *J. Am. Chem. Soc.*, 2005, **127**, 3366; Y. Cai, H. Pan, X. Xu, Q. Hu, L. Li and R. Tang, *Chem. Mater.*, 2007, **19**, 3081; Y. Zhao, Y. Xie, S. Yan and Y. Dong, *Cryst. Growth Des.*, 2009, **9**, 3072; T. Y. Cheang, S. M. Wang, Z. J. Hu, Z. H. Xing, G. Q. Chang, C. Yao, Y. Liu, H. Zhang and A. W. Xu, *J. Mater. Chem.*, 2010, **20**, 8050.
10 S. Collino, I. W. Kim and J. S. Evans, *Cryst. Growth Des.*, 2006, **6**, 839; I. W. Kim, E. DiMasi and J. S. Evans, *Cryst. Growth Des.*, 2004, **4**, 1113; C. Cheng, Y. Yang, X. Chen and Z. Shao, *Chem. Commun.*, 2008, 5511; C. Cheng, Z. Shao and F. Vollrath, *Adv. Funct. Mater.*, 2008, **18**, 2172; A. S. Deshpande and E. Beniash, *Cryst. Growth Des.*, 2008, **8**, 3084; C. Li, G. D. Botsaris and D. L. Kaplan, *Cryst. Growth Des.*, 2002, **2**, 387; F. Z. Cui, Y. Wang, Q. Cai and W. Zhang, *J. Mater. Chem.*, 2008, **18**, 3835.
11 P. Kasparov, M. Antonietti and H. Cöfen, *Colloids Surf., A*, 2004, **250**, 153; X. H. Guo, A. W. Xu and S. H. Yu, *Cryst. Growth Des.*, 2008, **8**, 1233.
12 X. H. Guo, S. H. Yu and G. B. Cai, *Angew. Chem., Int. Ed.*, 2006, **45**, 3977.
13 Y. Yao, W. Dong, S. Zhu, X. Yu and D. Yan, *Langmuir*, 2009, **25**, 13238.
14 T. Sugawara, Y. Suwa, K. Ohkawa and H. Yamamoto, *Macromol. Rapid Commun.*, 2003, **24**, 847.
15 D. Walsh, J. D. Hopwood and S. Mann, *Science*, 1994, **264**, 1576; H. T. Schmidt and A. E. Ostafin, *Adv. Mater.*, 2002, **14**, 532; C. Robinson, R. C. Shore, S. R. Wood, S. J. Brookes, D. A. M. Smith, J. T. Wright, S. Connell and J. Kirkham, *Connect. Tissue Res.*, 2003, **44**, 65; C. E. Fowler, M. Li, S. Mann and H. C. Margolis, *J. Mater. Chem.*, 2005, **15**, 3317.
16 L. Zhang and A. Eisenberg, *Science*, 1995, **268**, 1728; C. Cai, W. Zhu, T. Chen, J. Lin and X. Tian, *J. Polym. Sci., Part A: Polym. Chem.*, 2009, **47**, 5967; C. Cai, J. Lin, T. Chen, X. S. Wang and S. Lin, *Chem. Commun.*, 2009, 2709.
17 J. Rao, Z. Luo, Z. Ge, H. Liu and S. Liu, *Biomacromolecules*, 2007, **8**, 3871.
18 M. Antonietti, M. Breulmann, C. G. Göltner, H. Cölfen, K. K. W. Wong, D.Walsh and S. Mann, *Chem.–Eur. J.*, 1998, **4**, 2493.
19 W. Tjandra, J. Yao, P. Ravi, K. C. Tam and A. Alamsjah, *Chem. Mater.*, 2005, **17**, 4865.
20 Y. X. Gao, S. H. Yu, H. Cong, J. Jiang, A. W. Xu, W. F. Dong and H. Cölfen, *J. Phys. Chem. B*, 2006, **110**, 6432.
21 H. J. Lee, S. E. Kim, I. K. Kwon, C. Park, C. Kim, J. Yang and S. C. Lee, *Chem. Commun.*, 2010, **46**, 377.
22 M. G. Page, N. Nassif, H. G. Börner, M. Antonietti and H. Cölfen, *Cryst. Growth Des.*, 2008, **8**, 1792; Y. Y. Kim, K. Ganesan, P. Yang, A. N. Kulak, S. Borukhin, S. Pechook, L. Ribeiro, R. Kröger, S. J. Eichhorn, S. P. Armes, B. Pokroy and F. C. Meldrum, *Nat. Mater.*, 2011, **10**, 890.
23 Y. Y. Kim, A. N. Kulak, Y. Li, T. Batten, M. Kuball, S. P. Armes and F. C. Meldrum, *J. Mater. Chem.*, 2009, **19**, 387.
24 E. R. Blout and R. H. Karlson, *J. Am. Chem. Soc.*, 1956, **78**, 941.
25 G. Chen and A. S. Hoffman, *Nature*, 1995, **373**, 49.
26 C. Cai, L. Zhang, J. Lin and L. Wang, *J. Phys. Chem. B*, 2008, **112**, 12666; J. Rodríguez-Hernández and S. Lecommandoux, *J. Am. Chem. Soc.*, 2005, **127**, 2026.
27 S. Albeck, S. Weiner and L. Addadi, *Chem.–Eur. J.*, 1996, **2**, 278.
28 I. W. Kim, R. E. Robertson and R. Zand, *Cryst. Growth Des.*, 2005, **5**, 513.
29 S. H. Yu, H. Cölfen and M. Antonietti, *J. Phys. Chem. B*, 2003, **107**, 7396; S. H. Yu, H. Cölfen, J. Hartmann and M. Antonietti, *Adv. Funct. Mater.*, 2002, **12**, 541.

30 A. N. Kulak, P. Iddon, Y. Li, S. P. Armes, H. Cölfen, O. Paris, R. M. Wilson and F. C. Meldrum, *J. Am. Chem. Soc.*, 2007, **129**, 3729.
31 W. Li and P. Wu, *CrystEngComm*, 2009, **11**, 2466.
32 M. F. Butler, N. Glaser, A. C. Weaver, M. Kirkland and M. Heppenstall-Butler, *Cryst. Growth Des.*, 2006, **6**, 781.
33 F. A. Andersen and L. Brecevic, *Acta Chem. Scand.*, 1991, **45**, 1018.
34 R. L. Penn and J. F. Banfield, *Geochim. Cosmochim. Acta*, 1999, **63**, 1549.
35 S. H. Yu, H. Cölfen, K. Tauer and M. Antonietti, *Nat. Mater.*, 2005, **4**, 51.
36 S. Wohlrab, H. Cölfen and M. Antonietti, *Angew. Chem., Int. Ed.*, 2005, **44**, 4087.
37 R. S. K. Lam, J. M. Charnock, A. Lennie and F. C. Meldrum, *CrystEngComm*, 2007, **9**, 1226.
38 S. J. Homeijer, M. J. Olszta, R. A. Barrett and L. B. Gower, *J. Cryst. Growth*, 2008, **310**, 2938.
39 S. R. Dickinson, G. E. Henderson and K. M. McGrath, *J. Cryst. Growth*, 2002, **244**, 369; S. R. Dickinson and K. M. McGrath, *J. Mater. Chem.*, 2003, **13**, 928.
40 B. Pokroy and E. Zolotoyabko, *Chem. Commun.*, 2005, 2140; A. W. Xu, W. F. Dong, M. Antonietti and H. Cölfen, *Adv. Funct. Mater.*, 2008, **18**, 1307; N. Nassif, N. Gehrke, N. Pinna, N. Shirshova, K. Tauer, M. Antonietti and H. Cölfen, *Angew. Chem., Int. Ed.*, 2005, **44**, 6004.